Chip

Research Article

PHOTONICS

DOI: 10.1016/j.chip.2023.100043

On-chip photonic spatial-temporal descrambler

Wenkai Zhang[1], Xueyi Jiang[1], Wentao Gu[1], Junwei Cheng[1], Hailong Zhou[1,*], Jianji Dong[1,2], Dongmei Huang[3,4] & Xinliang Zhang[1,2]

[1]*Wuhan National Laboratory for Optoelectronics, Huazhong University of Science and Technology, Wuhan 430074, China* [2]*Optics Valley Laboratory, Wuhan 430074, China* [3]*The Hong Kong Polytechnic University Shenzhen Research Institute, Shenzhen 518057, China* [4]*Photonics Research Institute, Department of Electrical Engineering, The Hong Kong Polytechnic University, Hong Kong 999077, China*

E-mail: hailongzhou@hust.edu.cn (Hailong Zhou)

Cite as: Zhang, W. et al. *Chip* **2**, 100043 (2023).
https://doi.org/10.1016/j.chip.2023.100043

Received: 13 December 2022

Accepted: 1 March 2023

Published online: 7 March 2023

As an indispensable part to compensate for the signal crosstalk in fiber communication systems, conventional digital multi-input multi-output (MIMO) signal processor is facing the challenges of high computational complexity, high power consumption and relatively low processing speed. The optical MIMOenables the best use of light and has been proposed to remedy this limitation. However, the currently existing optical MIMO methods are all restricted to the spatial dimension, while the temporal dimension is neglected. Here, an on-chip spatial-temporal descrambler with four channels were devised and its MIMO functions were experimentally verified simultaneously in both spatial and temporal dimensions. The spatial crosstalk of single-channel descrambler and four-channel descrambler is respectively less than -21 dB and -18 dB, and the time delay is simultaneously compensated successfully. Moreover, a more universal model extended to mode-dependent loss and gain (MDL) compensation was further developed, which is capable of being cascaded for the real optical transmission system. The first attempt at photonic spatial-temporal descrambler enriched the varieties of optical MIMO, and the proposed scheme provided a new opportunity for all-optical MIMO signal processing.

Keywords: Optical signal processing, Photonic integrated circuits, Optical MIMO, Optical matrix computing

INTRODUCTION

Mode-division multiplexing (MDM) technology has been regarded as a promising way to meet the exponentially increasing demand for transmission capacity over decades[1–3]. When multiple modes propagate in the fiber, coupling inevitably occurs between different modes, which directly results in the crosstalk, and will seriously degrade the quality of signals. To address the critical issue above, the multi-input multi-output (MIMO) digital signal processing was introduced to compensate for the crosstalk of signals[4–6], while facing the challenges of high computational complexity and high power consumption, especially when the number of channels increases[7–9]. And the processing speed is greatly restricted by the digital devices, which leads to a large delay. With the maturity of large-scale optical integration technology, light has gradually become a potential alternative to break through the speed and power limitation of conventional electronic hardware both in optical neural networks and optical signal processing[10–13]. Numerous on-chip optical MIMO schemes have been proposed in recent years. The basic principle is to execute the inverse matrix of signal transmission coupling matrix through integrated optical methods such as Mach–Zehnder interferometer (MZI) meshes[14–18] and multi-plane light conversion[19–21]. As the light propagates through the chip, the chaotic signals can be recovered at the speed of light and only little energy is required to maintain the chip operating in the desired state. However, all the existing optical MIMO methods are restricted to the spatial dimension while the temporal dimension is neglected. Since the modes exhibit different propagation velocities in the fiber, the modal group delay (GD) associated with modal dispersion (MD) is generated accordingly, which is not conducive to the quality of signals when accompanying with the spatial coupling. Therefore, both spatial and temporal dimensions are supposed to be taken into consideration by the optical MIMO, which will compensate for the crosstalk as much as possible.

In the current work, an on-chip photonic spatial-temporal descrambler with four channels was put forward and its MIMO functions were experimentally verified using 25 Gbps on-off keying (OOK) signals. The descrambler is composed of two 4 × 4 optical unitary matrix units based on MZI meshes[22] for spatial decoupling and optical delay lines with different lengths for time delay compensation. In virtue of gradient descent algorithm in our previous works[18,21,23,24], the descrambler can be optimized to the desired state without any inner information. The spatial crosstalk and time delay are compensated simultaneously. In allusion to the real optical transmission systems, a more general optical MIMO model, which is cascadable and compensable for mode-dependent loss and gain (MDL), was further discussed. For the first time, the compensation for time delays of the signals and spatial coupling has been realized simultaneously, which marks a significant step to photonic spatial-temporal descrambler.

RESULTS

MDM matrix transmission model Fig. 1 shows the matrix propagation model of MDM transmission system, which can be divided into K cascaded sections[25–27]. For kth section, the transmission matrix in the frequency domain can be written by the following equation:

$$H^{(k)}(\omega) = V^{(k)} \cdot \Lambda^{(k)}(\omega) \cdot U^{(k)*}, \quad (1)$$

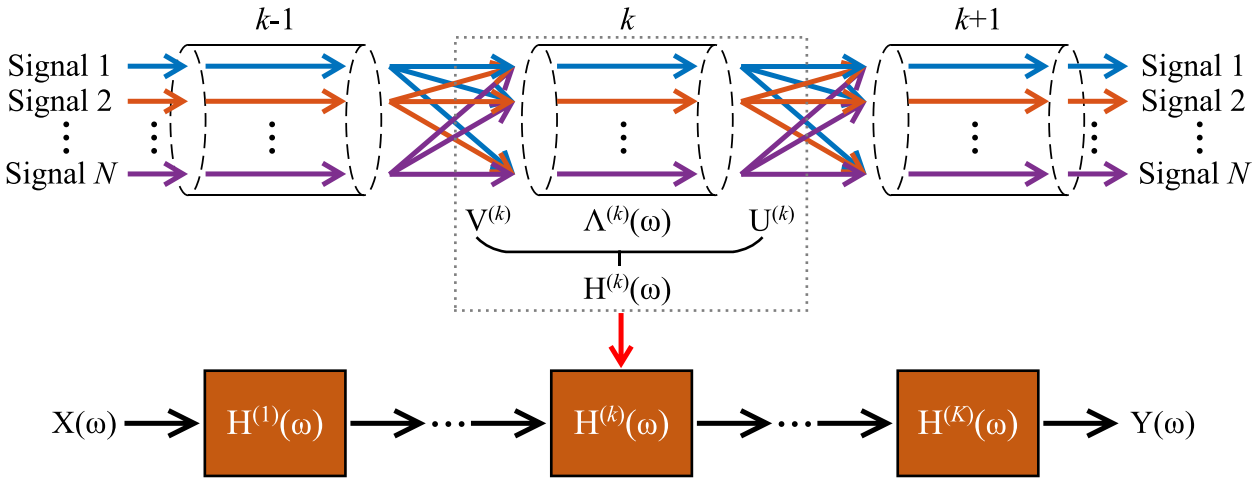

Fig. 1 | Matrix propagation model of MDM transmission system.

where, $V^{(k)}$ and $U^{(k)}$ denote the unitary coupling matrices inserted at the input and output of the kth section, respectively, and * represents the Hermitian transpose. When only considering the modal GD, the diagonal matrix $\Lambda^{(k)}$ can be expressed as:

$$\Lambda^{(k)}(\omega) = \begin{bmatrix} e^{-j\omega\tau_1^{(k)}} & \cdots & 0 \\ \vdots & \ddots & \vdots \\ 0 & \cdots & e^{-j\omega\tau_n^{(k)}} \end{bmatrix}, \tag{2}$$

where, τ_n^k represents the nth mode's group delay in kth section[25]. And the total transmission matrix can be given by:

$$H(\omega) = \prod_{k=1}^{K} H^{(k)}(\omega). \tag{3}$$

In the frequency domain, the input multichannel signals are defined by $X(\omega)$=$[X_1(\omega), X_2(\omega), \ldots, X_n(\omega)]^{\mathrm{T}}$, and the output signals by $Y(\omega)$= $[Y_1(\omega), Y_2(\omega), \ldots, Y_n(\omega)]^{\mathrm{T}}$. The relationship between the input and output signals of the MDM system can be expressed by:

$$Y(\omega) = H(\omega)X(\omega). \tag{4}$$

From Eqs. (1)–(4), it could be found that the modal GD acts as the time delay of different signals in each section. Therefore, it can be compensated by adding optical circuits with inverse lengths. Similarly, the coupling matrices can be compensated by inverse spatial matrix transmission with optical methods.

Principle of spatial-temporal descrambler For simplicity, one section of MDM matrix propagation model was taken to verify the function of the photonic spatial-temporal descrambler. As depicted in Fig. 2a, the proposed chip consists of two parts. One part is to introduce the spatial and temporal disorder according to the matrix model. It is composed of two spatial cross units which use directional couplers with the length of 100 μm and the waveguide interval of 0.2 μm, and a time delay unit between them adopting equidifferent optical paths with the length differenceof 1229 μm, corresponding to about 10 ps time delay (the n_{eff} of 500 nm width Si waveguide we use is 2.441). Another part is the spatial-temporal descrambler core, wherein the two 4 × 4 unitary MZI matrix units are designed to descramble the spatial disorder, and the inverse equidifferent optical paths are utilized for time compensation. The packaged chip and microscope image of the chip are shown in Fig. 2b and c, which was fabricated on a silicon-on-insulator (SOI) wafer with 220-nm-thick top silicon and 2-μm-thick buried oxide layer. Each of the 4 × 4 MZI matrix units is composed of 6 MZIs, to perform an arbitrary unitary transformation by tuning the phase shifters. The coupling loss at the wavelength of 1550 nm is about 3.9 dB, and the on-chip loss without coupling gratings is about 8 dB after configured.

The proposed spatial-temporal descrambler needs to configure the phase shifters in MZI meshes to the desired states. In the current work, the gradient descent algorithm was adopted to adjust each heater's voltage, which can be optimized by itself without any inner information[18,21,23,24]. of the crosstalk from both spatial and temporal dimensions, two cost functions (CFs) were adopted to evaluate the performances in spatial and temporal dimensions, respectively. and then use the product of them as the final CF. For N channels' spatial descrambling, the CF_{space} is defined as:

$$CF_{space} = \prod_{n=1}^{N} \frac{|P_n^{real} \cdot P_n^{tgt}|}{\|P_n^{real}\| \|P_n^{tgt}\|}, \tag{5}$$

where, $\prod$ is the scalar product of two vectors, $||$ is to get the absolute value, $\|\|$ is 2-norm of the vector, P_n^{real} is the optical power vector for all output ports and P_n^{tgt} is the targeted vector (e.g. P_n^{tgt} can be [0,1,0,0] if the signal is set to output from the Port 2.) when the signal is incident on the n-th input port. The CF_{space} denotes the correlation between the real and targeted results, which ranges from 0 to 1. And the closer to 1 the CF is, the more relevant the real and targeted results will be.

As for time compensation, the correlation between input and output waveforms was also exploited and used as the evaluation criterion. The waveform collected by optical oscilloscope (OSC) are made up of discrete points, which can be seen as a waveform vector. And the correlation can be calculated by the following equation:

$$Corr(m_1, m_2) = \frac{|W^{real}[m_1 : (m_1 + m_T)] \cdot W^{tgt}[m_2 : (m_2 + m_T)]|}{\|W^{real}[m_1 : (m_1 + m_T)]\| \|W^{tgt}[m_2 : (m_2 + m_T)]\|}, \tag{6}$$

where, W^{real} and W^{tgt} denote the input and output waveform vectors, respectively. In Eq. (6), we take the points from m_1 to $m_1 + m_T$ in W^{real} and the points from m_2 to $m_2 + m_T$ in W^{tgt}, where, m_T is the number of points in one period of the waveform. In some cases, the input and output signals are not precisely aligned in time. Therefore, in order to get the time cost function CF_{time}, it is needed to find out the most matched time point to calculate the correlation, which corresponds to searching for the maximum correlation when m_1 changes in one period of the signal. This process can

DOI: 10.1016/j.chip.2023.100043

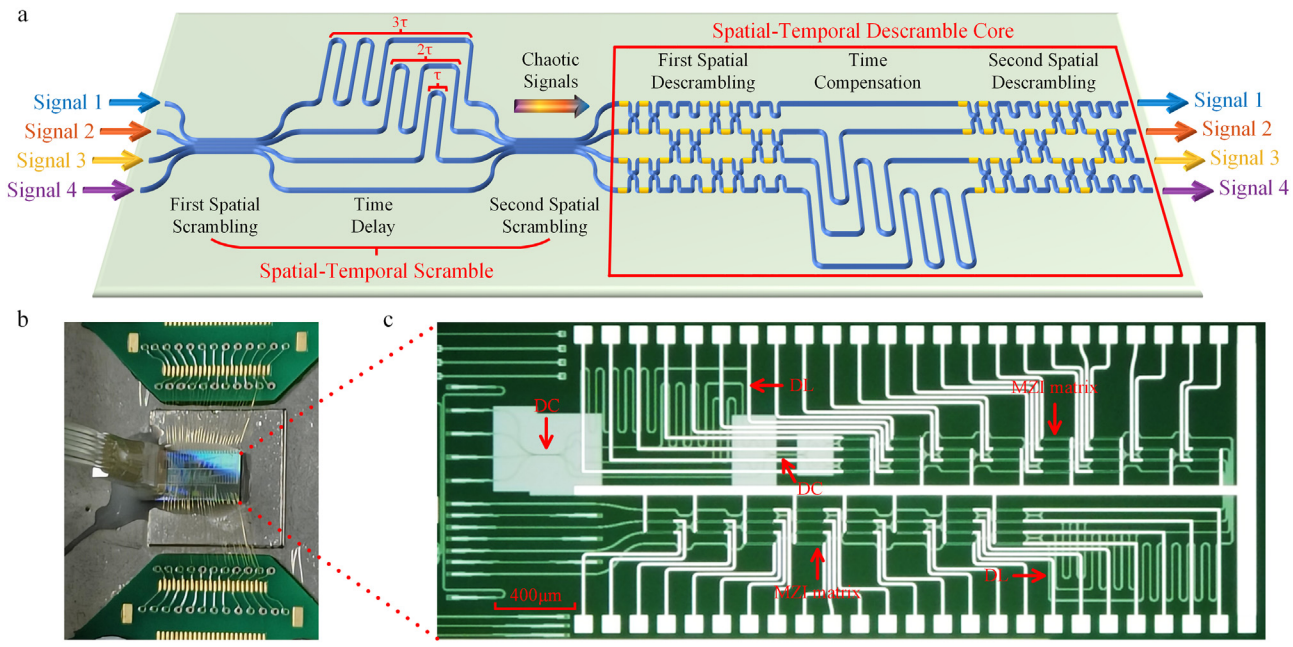

Fig. 2 | Design of the spatial-temporal descrambler. a, Schematic diagram of the spatial-temporal descrambler chip. **b,** Photograph of the packaged chip. **c,** Microscope image of the spatial-temporal descrambler chip. DC, directional coupler; DL, delay lines.

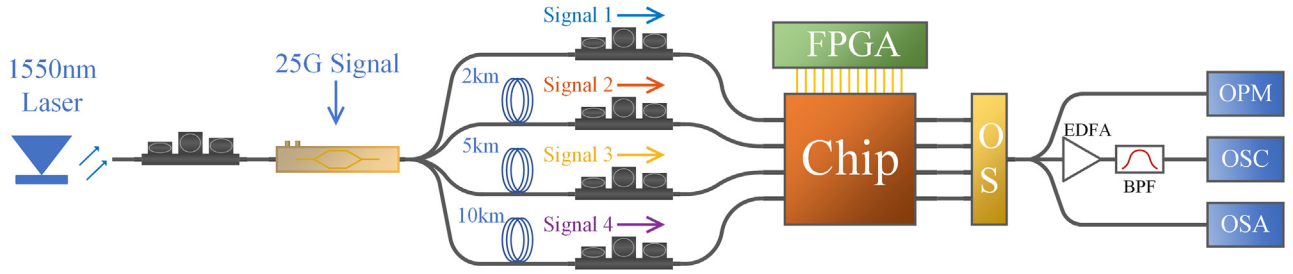

Fig. 3 | Experimental setup of the spatial-temporal descrambler. FPGA, field programmable gate array. OS, optical switch; EDFA, erbium doped fiber amplifier; BPF, bandpass filter; OPM, optical power monitor; OSC, optical oscilloscope; OSA, optical spectrum analyzer.

be expressed as:

$$CF_{time} = \prod_{n}^{N} \max_n[Corr(m_1, m_2), Corr(m_1 + 1, m_2), \ldots, Corr(m_1 + m_T - 1, m_2)], \quad (7)$$

where, $\max_n$ represents the maximum correlation between input and output waveforms when the signal is incident in the n-th channel. After obtaining the cost functions of space and time, the total cost function CF_{total} is defined by:

$$CF_{total} = CF_{space} \cdot CF_{time} \quad (8)$$

With the aid of gradient descent algorithm, the CF_{total} can be improved by altering the voltage of the heaters. As CF_{total} gets closer to 1, the voltage change step is gradually decreased to guarantee that the MZI matrices are well optimized. At the end of the iteration, the signals can be descrambled both in spatial and temporal dimensions.

Experimental setup and results As shown in Fig. 3, a 25 Gbps optical signal is generated by a lithium niobite MZI intensity modulator (IM) and divided into four channels by a 1 × 4 optical splitter. Single mode fibers of different lengths are introduced to decorrelate the signals of the four channels, differential time delays of which are much greater than the coherence length of the laser. Then the four signals are incident into the input ports of chip and the results from output ports can be chosen via optical switch. During the configuration state, the periodic signal of 400 ps (10 bits, 40 ps per bit) is loaded into the IM and guides the descrambler to optimize in the temporal dimension. And the field programmable gate array (FPGA) is applied to control the voltage of the heaters according to the results detected by corresponding instruments.

One channel (input Port 3 to output Port 3) was firstly selected to validate the temporal descrambling function of the chip. As depicted in Fig. 4c, the crosstalk in temporal dimension can be easily found from the broadening and distortion of the initial output waveform. And the mixing eye diagram demonstrates that the temporal crosstalk could exert greatlinfluence on the quality of the signals. Note that the delay of signal may be greater than 30 ps before optimization of the spatial-temporal descrambler, which is mainly ascribed to the fact that the time compensation part is also likely to introduce time delay. Fig. 4a and Fig. 4b present the evolution process of the descrambler during the optimization in spatial (making the power of targeted output port maximal) and temporal dimension, respectively. In one iteration, one of the MZIs' heaters was selected in sequence to change the applied voltage. If the CF_{total} in Eq. (8) increases, the voltage change is maintained, if not, the original voltage is turned back. The

DOI: 10.1016/j.chip.2023.100043

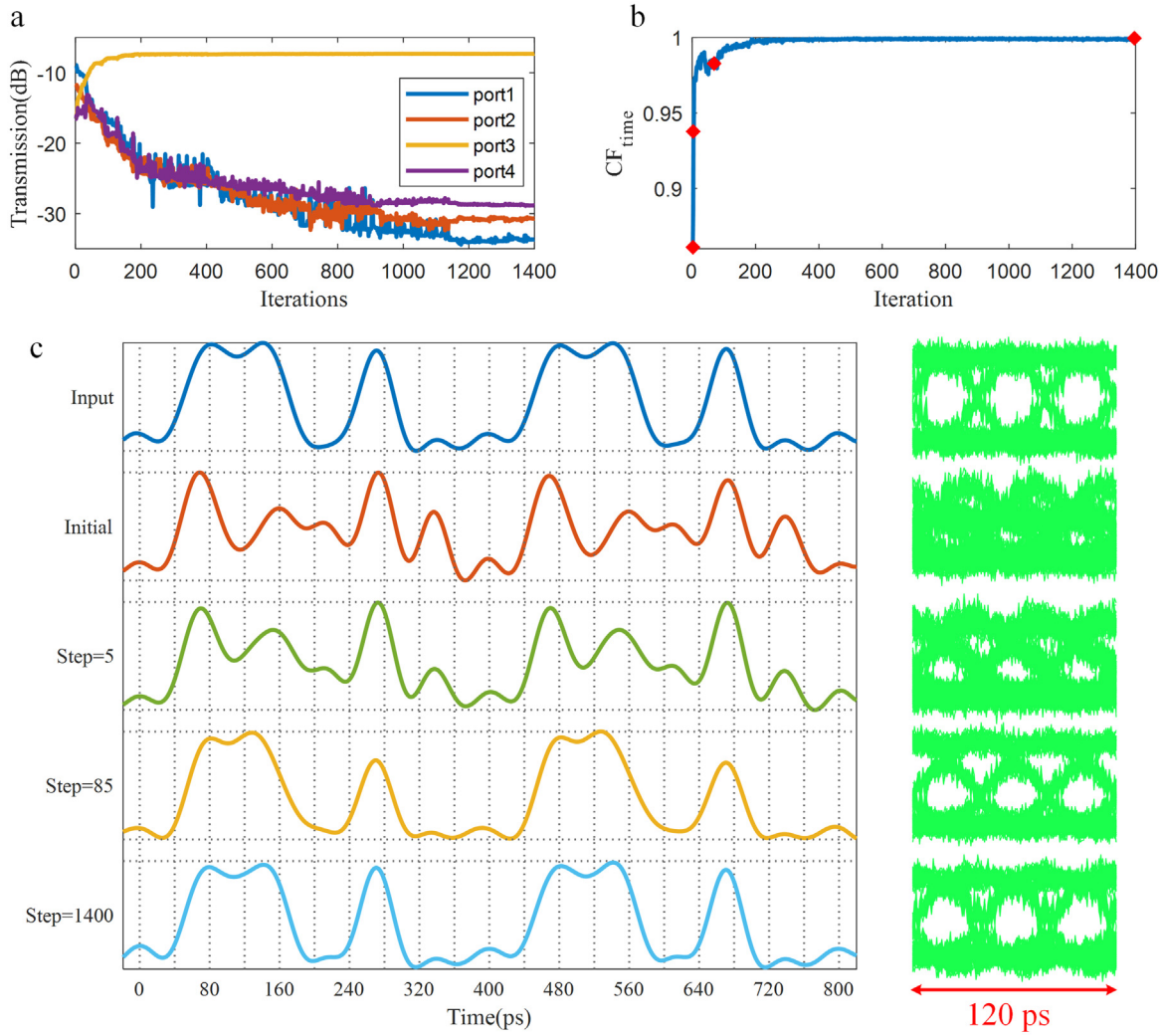

Fig. 4 | Experimental results of one channel's spatial-temporal descramble. a, The power transmission of four output ports during the iteration. **b,** The CF_{time} versus optimization iteration. **c**, Waveforms and eye diagrams of input signal and output signals at the step of 1 (initial results), 5, 85 and 1400 (final results).

voltage change is firstly set to 100 mV, and gradually decreased to 10 mV to realize more refined optimization during the evolution. The extinction ratio (ER) between the selected port and other ports increases gradually, and the waveform and the eye diagram in Fig. 4c are also improved. Under the iteration number of around 400, the CF in temporal dimension is close to its best, while further optimization is required for the ER. After 1400 iterations, the correlation between input and output signals reaches 0.999 and the minimum ER (Port 3 and Port 4) is about 21.57 dB, which reveals that the descrambler is capable of eliminating the crosstalk both in spatial and temporal dimensions.

In the further experiment, the capacity of the chip is explored to descramble four channels simultaneously. Fig. 5a-c show the three different routing states of the spatial-temporal descrambler. The final spatial crosstalk is less than 18 dB and the final wave correlations of four output ports all achieve 0.999. In the routing state depicted in Fig. 5c, the descramblers' transmission spectrums (Fig. 5d) are measured with a broadband light source. It is the optical paths of equal length difference that induce the periodic resonance peaks in the transmission curves, which is like the spectrums of optical delay interferometer. And the eye diagrams of four output ports in Fig. 5e also illustrate the success of spatial-temporal descramble.

DISCUSSION

The above results fully demonstrated the capacity of spatial-temporal descrambler for the proposed chips. Despite the proof-of-principle verification of spatial-temporal descrambler, the first attempt at spatial-temporal compensation broke through the confinement of the existing optical MIMOs which only realize spatial descrambling. For further perfection of the proposed scheme, it's necessary to take the MDL into consideration, in which the mode-dependent loss is introduced by fibers or passive components, and mode-dependent gain can be generated by multimode optical amplifiers[26,27]. In this case, the $\Lambda^{(k)}$ in Eq. (2) is composed of the power matrix $P^{(k)}(\omega)$ and time matrix $T^{(k)}(\omega)$, rewritten as:

$$\begin{aligned}\Lambda^{(k)}(\omega) &= P^{(k)}(\omega)\cdot T^{(k)}(\omega)\\ &= \begin{bmatrix} e^{\frac{1}{2}g_1^{(k)}} & \cdots & 0 \\ \vdots & \ddots & \vdots \\ 0 & \cdots & e^{\frac{1}{2}g_n^{(k)}} \end{bmatrix}\cdot \begin{bmatrix} e^{-j\omega\tau_1^{(k)}} & \cdots & 0 \\ \vdots & \ddots & \vdots \\ 0 & \cdots & e^{-j\omega\tau_n^{(k)}} \end{bmatrix}\\ &= \begin{bmatrix} e^{\frac{1}{2}g_1^{(k)}-j\omega\tau_1^{(k)}} & \cdots & 0 \\ \vdots & \ddots & \vdots \\ 0 & \cdots & e^{\frac{1}{2}g_n^{(k)}-j\omega\tau_n^{(k)}} \end{bmatrix},\end{aligned} \tag{9}$$

DOI: 10.1016/j.chip.2023.100043

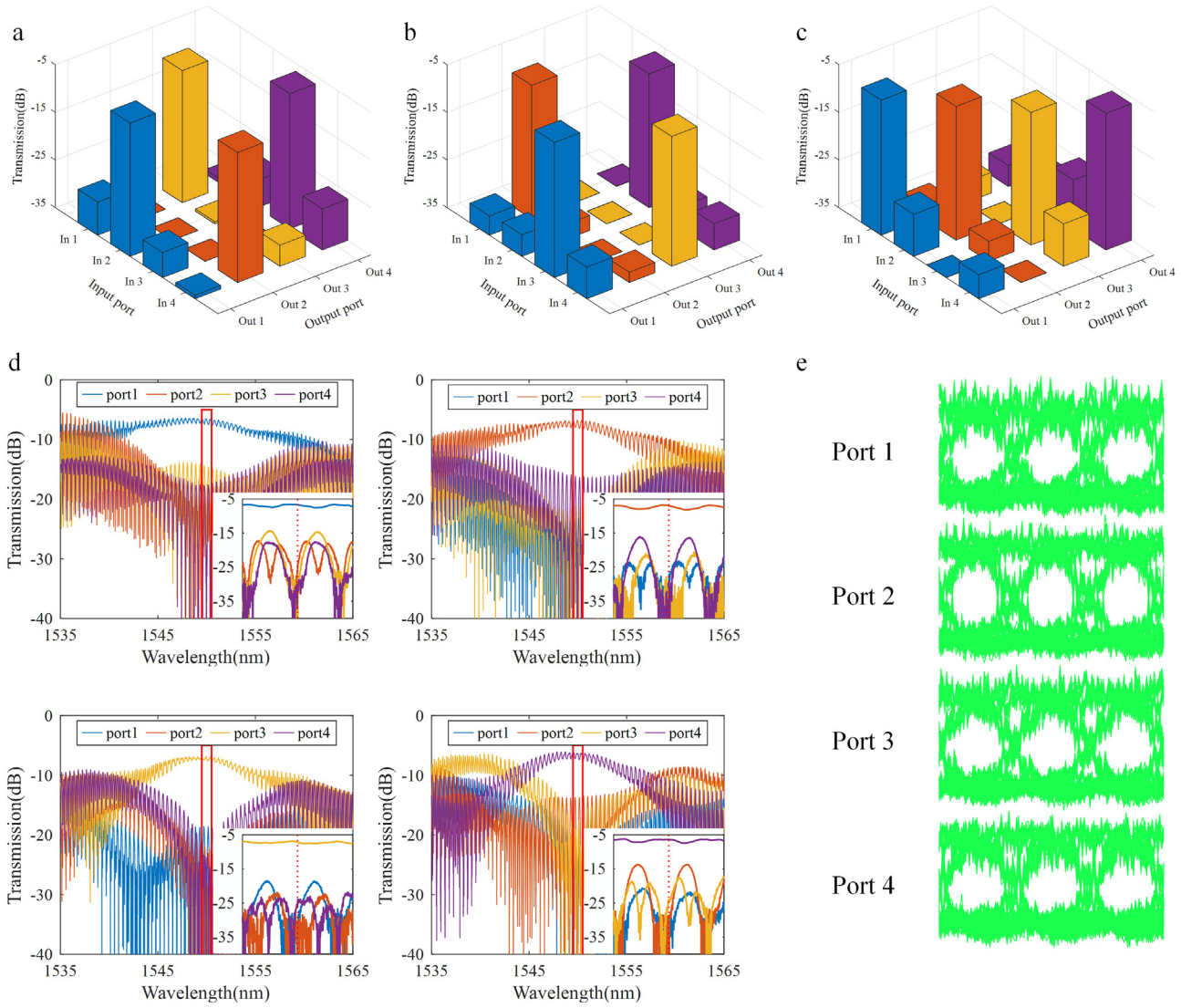

Fig. 5 | Experimental results of four channels' spatial-temporal descramble. a-c, Power transmission of the spatial-temporal descrambler in different routing states at the wavelength of 1550 nm. **d,** Spectrums of four output ports when the light is incident into input Port 1, Port 2, Port 3, and Port 4, respectively for the last routing state. The insets in the bottom right are the enlargements of spectrums from 1549.5 nm to 1550.5 nm. **e,** The final eye diagrams of the output ports when the signals are input into four channels.

where $g_n^{(k)}$ represents the nth mode's MDL in the kth section. As the MDL will lead to different power changes of each mode, the descrambler requires the power attenuators to balance the loss of each channel. According to Eq. (1) and Eq. (3), the $U^{(k)*}$ and $V^{(k+1)}$ can be combined by one unitary matrix of $M^{(k)}$and then the MDM transmission matrix of $H(\omega)$ is given by:

$$H(\omega) = \prod_{k=1}^{K} M^{(k)} \cdot \Lambda^{(k)}(\omega), \tag{10}$$

where $M^{(k)}$ denotes the unitary matrix of spatial coupling in the k-th section. In order to recover the input signals, the transmission matrix of optical MIMO is required to preform the inverse matrix of $H(\omega)$, which is expressed as:

$$H^{-1}(\omega) = \prod_{k=1}^{K} \left(\Lambda^{(K-k+1)}(\omega)\right)^{-1} \cdot \left(M^{(K-k+1)}\right)^{-1}. \tag{11}$$

In the light of Eq. (11), a universal optical MIMO model was constructed and depicted in Fig. 6(b), which was cascaded by multiple spatial-temporal descramblers. For kth section, the transmission matrix $D^{(k)}(\omega)$ of the descrambler is defined by:

$$\begin{aligned} D^{(\mathrm{k})}(\omega) &= \left(\Lambda^{(\mathrm{K-k+1})}(\omega)\right)^{-1}\left(M^{(\mathrm{K-k+1})}\right)^{-1} \\ &= \left(T^{(\mathrm{K-k+1})}(\omega)\right)^{-1}\left(P^{(\mathrm{K-k+1})}(\omega)\right)^{-1}\left(M^{(\mathrm{K-k+1})}\right)^{-1}. \end{aligned} \tag{12}$$

Specifically in terms of optical implementation, the descrambler can be divided into three parts: time compensation defined by $\left(T^{(K-k+1)}(\omega)\right)^{-1}$, power balance defined by $\left(P^{(K-k+1)}(\omega)\right)^{-1}$, and spatial descrambling defined by $\left(M^{(K-k+1)}\right)^{-1}$, as presented in Fig. 6a. The on-chip tunable delay lines can be employed for the time compensation[28–30], while the optical attenuators like MZI[31] or PIN structures[32] can form the power balance part. As for the spatial descrambling , the MZI matrix meshes are desirable for optical unitary conversion and capable of scaling to N channels[22,33]. All of these three parts are adjustable, making the

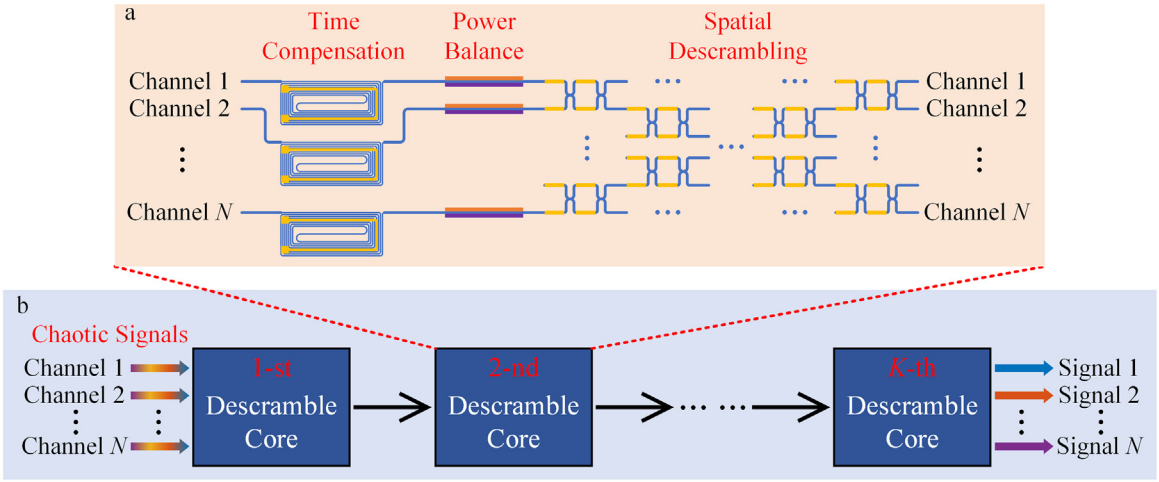

Fig. 6 | Sketch map of optical MIMO model. a, Detailed structure of the proposed spatial-temporal descrambler. **b,** Optical MIMO realized by cascaded spatial-temporal descramblers.

descrambler applicable to more scenarios. The low loss design of delay lines and MZIs is also worthy of being taken into consideration[34,35] and the erbium doped fiber amplifier can be inserted to guarantee sufficient descrambling sections for the optical MIMO cascade.. Since the signals are processed in the optical domain, and the descrambling speed is equal to that of the light, little energy is required to maintain the working state once configured. This cascadable model provides a sophisticated strategy of optical MIMO and can be further applied into the real optical transmission systems.

CONCLUSIONS

In the current work, an optical MIMO has been extended to both the spatial and temporal dimensions for the first time, and an on-chip spatial-temporal descrambler with four channels was experimentally demonstrated. With the aid of gradient descent algorithm, the chip could be configured to the targeted state by tuning the voltage of each heater . The spatial crosstalk is less than −18 dB for four-channel descrambler while ensuring the time recovery. Moreover, we discussed a more general optical descrambler which was capable of compensating for MDL and could be cascaded to form an optical MIMO for real fiber transmission systems. The proposed scheme is no longer confined to the spatial descrambling, and more dimensions (space, time and loss) are taken into consideration, which greatly broadens the range of the existing optical MIMO and will offer new opportunities for all-optical MIMO signal processing.

METHODS

Fabrication of the spatial-temporal descrambler chip The proposed chip was fabricated on a silicon-on-insulator (SOI) wafer with 220-nm-thick top silicon and 2-μm-thick buried oxide layer. The Si waveguide is 220 nm thick strip waveguide, while the grating coupler is fan-shaped with 70 nm shallow etch.The structure was patterned to photoresist adopting 248 nm deep UV lithography, followed by 70 nm partial grating etch. The remaining part of strip waveguide was then patterned and etched to BOX. Thereafter, Plasma Enhanced Chemical Vapor Deposition (PECVD) was introduced to deposit 1.2 μm pad oxide between Si waveguides and microheaters. Then a layer of 120 nm thick TiN was deposited and etched as the heater layer. Each heater unit is 150 μm long and 2.2 μm wide. Afterwards, Al was deposited and etched to form the metal wires and pads. The SOI chip was then glued on a ceramic-wafer printed circuit and the pads were wire-bonded to the printed circuit board. And the chip size is about 4.5 mm x 1.7 mm.

REFERENCES

1. Richardson, D.J., Fini, J.M., & Nelson, L.E. Space-division multiplexing in optical fibres. *Nat. Photonics* **7**, 354-362 (2013). https://doi.org/10.1038/nphoton.2013.94.
2. Li, G., Bai, N., Zhao, N. & Xia, C. Space-division multiplexing: the next frontier in optical communication. *Adv. Opt. Photonics* **6**, 413487 (2014). https://doi.org/10.1364/AOP.6.000413.
3. Puttnam, B. J., Rademacher, G. & Luis, R. S. Space-division multiplexing for optical fiber communications. *Optica* **8**, 1186–1203 (2021). https://doi.org/10.1364/OPTICA.427631.
4. Randel, S. et al. 6×56-Gb/s mode-division multiplexed transmission over 33-km few-mode fiber enabled by 6×6 MIMO equalization. *Opt. Express* **19**, 16697–16707 (2011). https://doi.org/10.1364/OE.19.016697.
5. Randel, S. et al. First real-time coherent MIMO-DSP for six coupled mode transmission. In *2015 IEEE Photonics Conference (IPC)*. (IEEE, 2015). https://doi.org/10.1109/IPCon.2015.7323761.
6. Beppu, S. et al. Real-time strongly-coupled 4-core fiber transmission. In *Optical Fiber Communication Conference (OFC) 2020*. (OSA Technical Digest, Th3H.2 Optica, 2020). https://doi.org/10.1364/OFC.2020.Th3H.2.
7. Arik, S. Ö., Askarov, D. & Kahn, J. M. Effect of mode coupling on signal processing complexity in mode-division multiplexing. *J. Light. Technol.* **31**, 423–431 (2012). https://doi.org/10.1109/JLT.2012.2234083.
8. Inan, B. et al. DSP complexity of mode-division multiplexed receivers. *Opt. Express* **20**, 10859–10869 (2012). https://doi.org/10.1364/OE.20.010859.
9. Diamantopoulos, N. P., Shariati, B. & Tomkos, I. On the power consumption of MIMO processing and its impact on the performance of SDM networks. In *2017 Optical Fiber Communications Conference and Exhibition (OFC)*, 1–3 (IEEE, 2017). https://ieeexplore.ieee.org/abstract/document/7936965.
10. Bogaerts, W. et al. Programmable photonic circuits. *Nature* **586**, 207–216 (2020). https://doi.org/10.1038/s41586-020-2764-0.
11. Shastri,B. J. et al. Photonics for artificial intelligence and neuromorphic computing. *Nat. Photonics* **15**, 102–114 (2021). https://doi.org/10.1038/s41566-020-00754-y.
12. Li, C., Zhang, X., Li, J., Fang, T. & Dong, X. The challenges of modern computing and new opportunities for optics. *PhotoniX* **2**, 20 (2021). https://doi.org/10.1186/s43074-021-00042-0.
13. Zhou, H. et al. Photonic matrix multiplication lights up photonic accelerator and beyond. *Light Sci. Appl.* **11**, 30 (2022). https://doi.org/10.1038/s41377-022-00717-8.
14. Doerr, C. R. Proposed architecture for MIMO optical demultiplexing using photonic integration. *IEEE Photonics Technol. Lett.* **23**, 1573–1575 (2011). https://doi.org/10.1109/LPT.2011.2164061.
15. Fontaine, N. K. et al. Space-division multiplexing and all-optical MIMO demultiplexing using a photonic integrated circuit. In *2012 OFC/NFOEC*, 1–3 (IEEE, 2012). https://ieeexplore.ieee.org/abstract/document/6192240.
16. Miller, D. A. B. Reconfigurable add-drop multiplexer for spatial modes. *Opt. Express* **21**, 20220–20229 (2013). https://doi.org/10.1364/OE.21.020220.

17. Annoni, A. et al. Unscrambling light—automatically undoing strong mixing between modes. *Light Sci. Appl.* **6**, e17110 (2017). https://doi.org/10.1038/lsa.2017.110.
18. Zhou, H. et al. All-in-one silicon photonic polarization processor. *Nanophotonics* **8**, 2257–2267 (2019). https://doi.org/10.1515/nanoph-2019-0310.
19. Tang, R., Tanemura, T. & Nakano, Y. Integrated reconfigurable unitary optical mode converter using MMI couplers. *IEEE Photonics Technol. Lett.* **29**, 971–974 (2017). https://doi.org/10.1109/LPT.2017.2700619.
20. Tang, R. et al. Reconfigurable all-optical on-chip MIMO three-mode demultiplexing based on multi-plane light conversion. *Opt. Lett.* **43**, 1798–1801 (2018). https://doi.org/10.1364/OL.43.001798.
21. Cheng, J. et al. Photonic Emulator for Inverse Design. *ACS Photonics* (accepted, 2022). https://doi.org/10.1021/acsphotonics.2c00716.
22. Clements, W. R., Humphreys, P. C., Metcalf, B. J., KolthammerI, W. S. & Walmsley, I. A. Optimal design for universal multiport interferometers. *Optica* **3**, 1460–1465 (2016). https://doi.org/10.1364/OPTICA.3.001460.
23. Zhou, H. et al. Chip-scale optical matrix computation for PageRank algorithm. *IEEE J. Sel. Top. Quantum Electron.* **26**, 8300910 (2019). https://doi.org/10.1109/JSTQE.2019.2943347.
24. Zhou, H. et al. Self-configuring and reconfigurable silicon photonic signal processor. *ACS Photonics* **7**, 792–799 (2020). https://doi.org/10.1021/acsphotonics.9b01673.
25. Ho, K.-P. & Kahn, J. M. Statistics of group delays in multimode fiber with strong mode coupling. *J. Light. Technol.* **29**, 3119–3128 (2011). https://doi.org/10.1109/JLT.2011.2165316.
26. Ho, K.-P. & Kahn, J. M. Mode-dependent loss and gain: statistics and effect on mode-division multiplexing. *Opt. Express* **19**, 16612–16635 (2011). https://doi.org/10.1364/OE.19.016612.
27. Ho, K.-P. & Kahn, J. M. *Mode Coupling and its Impact on Spatially Multiplexed Systems.* In *Optical Fiber Telecommunications (Sixth Edition)*, 491–568. (Academic Press, 2013). https://doi.org/10.1016/B978-0-12-396960-6.00011-0.
28. Lee, H., Chen, T., Li, J., Painter, O. & Vahala, K. J. Ultra-low-loss optical delay line on a silicon chip. *Nat. Commun.* **3**, 867 (2012). https://doi.org/10.1038/ncomms1876.
29. Wang, X. et al. Continuously tunable ultra-thin silicon waveguide optical delay line. *Optica* **4**, 507–515 (2017). https://doi.org/10.1364/OPTICA.4.000507.
30. Ji, X. et al. On-chip tunable photonic delay line. *APL Photonics* **4**, 090803 (2019). https://doi.org/10.1063/1.5111164.
31. Watanabe, K. et al. Ultralow power consumption silica-based PLC-VOA/switches. *J. Light. Technol.* **26**, 2235–2244 (2008). https://doi.org/10.1109/JLT.2008.920542.
32. Yuan, P., Wu, Y.-D., Wang, Y., An, J.-M. & Hu, X.-W. A fast SOI-based variable optical attenuator with a pin structure with low polarization dependent loss. *Optoelectron. Lett.* **12**, 20–22 (2016). https://doi.org/10.1007/s11801-016-5234-z.
33. Reck, M., Zeilinger, A., Bernstein, H. J. & Bertani, P. Experimental realization of any discrete unitary operator. *Phys. Rev. Lett.* **73**, 58 (1994). https://doi.org/10.1103/PhysRevLett.73.58.
34. Thomson, J. D., Hu, Y., Reed, G. T. & Fedeli, J.-M. Low loss MMI couplers for high performance MZI modulators. *IEEE Photonics Technol. Lett.* **22**, 1485–1487 (2010). https://doi.org/10.1109/LPT.2010.2063018.
35. Heck, M. J. R., Bauters, J. F., Davenport, M. L., Spencer, D. T. & Bowers, J. E. Ultra-low loss waveguide platform and its integration with silicon photonics. *Laser Photonics Rev.* **8**, 667–686 (2014). https://doi.org/10.1002/lpor.201300183.

MISCELLANEA

Author contributions H.Z. and W.Z. conceived the idea. W.Z. designed and fabricated the spatial-temporal descramble chip. W.Z., X.J. and W.G. designed and performed the experiments. J.D., H.Z., W.Z., and J.C. discussed and analyzed the data. W.Z. and H.Z prepared the manuscript, J.D. and D.H. revised the paper, and X.Z. supervised the project. All authors contributed to the writing of the manuscript.

Data availability Data underlying the results presented in this paper are not publicly available at this time but may be obtained from the authors upon reasonable request.

Funding National Key Research and Development Program of China (2021YFB2801903, 2021YFB2801900); National Natural Science Foundation of China (62075075, U21A20511, 62275088); Innovation Project of Optics Valley Laboratory (Grant No. OVL2021BG001).

Declaration of Competing Interest The authors declare no competing interest.